RM No. E8E11

NACA

RESEARCH MEMORANDUM

RESIDUAL STRESS ANALYSIS OF OVERSPEEDED DISK WITH CENTRAL HOLE BY X-RAY DIFFRACTION

By James N. Good

Flight Propulsion Research Laboratory
Cleveland, Ohio

TECHNICAL EDITING WAIVED

NATIONAL ADVISORY COMMITTEE FOR AERONAUTICS

WASHINGTON

July 23, 1948

NACA RM No. E8E11

NATIONAL ADVISORY COMMITTEE FOR AERONAUTICS

RESEARCH MEMORANDUM

RESIDUAL STRESS ANALYSIS OF OVERSPEEDED DISK WITH CENTRAL HOLE BY X-RAY DIFFRACTION

By James N. Good

SUMMARY

An analysis was made of the residual surface stresses of a parallel-sided 3S-0 aluminum disk with a central hole after plastic strain had been introduced by centrifugal overspeed, that is, those speeds at which the elastic limit was exceeded, and by central compression. Improvements in camera equipment, X-ray - intensity control, and technique for photographic X-ray stress analysis developed at the NACA Cleveland laboratory were used with a microcomparator and microphotometer.

Locally high stress differences were found superimposed on an over-all trend in the stress curves measured on the surface of a disk overspeeded under conditions at which the surface stresses may have been different from the body stresses. Both the tangential and radial residual surface stresses from centrifugal plastic straining were tensile over the greatest portion of the disk radius even after 3 weeks. Fluctuations between high tensions and high compressions, however, were found in an area adjacent to the central hole.

Tangential residual surface stresses within a strain band near the central hole of a disk overspeeded under conditions at which the surface stresses were probably representative of the body stresses were highly compressive. These stresses were those that remained after the disk was subjected to centrifugal plastic straining by an unbalanced vibratory motion between the edge of the central hole and the driving mechanism. From the hole to the rim, the tangential stresses changed from compressive to tensile. The radial stress was compressive except for a region of highly tensile stress at three-quarters of the disk radius. Fluctuations were found in tensile stresses between adjacent circumferential points that were also located at three-quarters of the disk radius, but on a radius not in the strain band. The stresses at one-quarter of the disk radius on this radius were consistent and in fair agreement with those found at one-quarter of the disk radius in the strain band.

INTRODUCTION

The measurement of residual stresses after overspeed, that is, speeds at which the elastic limit of the disk material has been exceeded, is one of the problems encountered in the determination of the stresses in rotating disks. Because the residual stresses, as a first approximation, equal the difference between the elastic stresses and the plastic stresses (reference 1), the plastic operating stresses may be determined from them. True stresses, for example, that may have critical concentration resulting from anisotropy in the disks have, however, remained unknown. Although techniques for the determination of residual stresses in metals by strain gages and other methods are known, in most cases these methods are destructive to the material and have other limitations as well. It is therefore advantageous to use the nondestructive X-ray - diffraction method to measure surface stresses. Measurement of the residual-stress distribution in the surface of a parallel-sided disk that has a central hole is therefore a step in the experimental stress analyses of gas-turbine disks.

The well-known use of X-ray diffraction for stress measurement has the advantage of being the only experimental stress-measurement method operable without knowledge of the prior unstressed condition and it is the only completely nondestructive technique for measuring residual stresses. Application of the method to the determination of residual stresses in the high-temperature alloys used in gas-turbine disks may, however, offer difficulty. Accuracy of stress determinations by this method may be difficult or impossible to obtain under some conditions, for example, when such alloys are structurally deformed on an atomic scale. Aluminum, however, gives reasonably sharp diffraction lines in the plastic-flow condition.

In a preliminary investigation of the residual stresses at the surface of an overspeeded disk, which was conducted at the NACA Cleveland laboratory, maximum accuracy was sought through use of an aluminum disk. The disk was overspeeded, the residual stresses were measured, and the disk was annealed to relieve the stresses. The disk was overspeeded a second time for an intended higher speed and for measurement of the new residual stresses.

This investigation was conducted primarily to measure the effect of overspeed on the magnitude and the distribution of stresses in the surface of a flat, parallel-sided, ductile disk with a central hole. A secondary purpose was the improvement of the equipment and technique for X-ray - diffraction stress analysis to a more practical status.

APPARATUS AND PROCEDURE

The disk investigated was made from 3S-0 aluminum rolled stock, 5/8 inch thick, and was machined on both sides to 3/8-inch thickness to remove any surface contamination and variation in cross-sectional grain conditions introduced by rolling. The inside diameter of the disk was 2.75 inches and the outside diameter was 14.00 inches. The 3S-0 alloy was chosen because it would yield sharp diffraction patterns without the interference produced by alloying agents and without the inherently rapid self-annealing of pure aluminum at room temperature. The aluminum disk was fully annealed to remove any stresses in the material, metallurgically sanded to remove the worked layer, and macroetched in caustic. The etched surface is shown in figure 1.

The disk was spun in a vacuum spin pit comprising a steel-lined chamber with a cover plate to which were attached an air turbine and vacuum and oil lines. The disk-holding devices used were of the two types shown in figure 2. Type A (fig. 2(a)) was made of steel and was designed to introduce no compressive stresses at the disk center by the centrifugal force of "tulip petals" as in type B (fig. 2(b)). Type B was made of material soft enough to expand with the disk and was designed to introduce no possible surface-stress effects by clamping of plates against the surface (as in type A).

The X-ray measurements of the disk before overspeeding gave the unstressed spacing between the (420) planes. The disk was again X-rayed after having been spun at a rotor speed of 11,500 rpm with the type-A holding device, which produced an increase of 0.06 inch in the inside diameter and 0.04 inch in the outside diameter. As plastic flow began, the disk became slightly thinner at the center, was thereby relieved of any initial surface pressure by the clamping plates, and was left slightly loose and free to stretch. The disk was reannealed, mounted on a type-B holding device, and spun for an intended higher speed. At 10,000 rpm, however, an unbalance developed when the tulip failed to expand with the disk, at which point the run was discontinued. The unbalanced motion of the disk compressed the material adjacent to the central hole, which was enlarged 1/4 inch without change in the outside diameter. Inasmuch as there was no change in the outside diameter, the elastic limit in tension was not exceeded over the outer radial portion of the disk.

X-ray - diffraction examination of the spun specimens was made using a portable two-window cobalt X-ray tube of the permanent-vacuum type, operated at 35 kilovolts and 11 milliamperes. An automatic current controller, which was designed and built at the Cleveland laboratory, was used to maintain the X-ray current, and

consequently the X-ray intensity, constant at the full rated value during the full period of exposure. This controller relieved the operator of the intermittent manual adjustment usually necessitated by the 10- to 15-percent drop in the current that occurs during the early part of each operational period. The operating arrangement of X-ray camera, portable tube and stand, power unit, current controller, and automatic timer is shown in figure 3. A special back-reflection camera, so designed and constructed as to permit installation very close to the X-ray tube, made possible the use of short exposure times. The whole camera-and-tube assembly was so designed and fabricated as to allow rapid change in camera position and in angle of X-ray incidence to the disk. A small reversible motor was mounted on the camera with an automatic microswitch and relay controllers. The camera could be continuously rotated clockwise or could be oscillated $\pm 30^{\circ}$ at 1 rpm.

All X-ray exposures, which were 10 or 15 minutes long, were made with a collimated beam 1/32 inch in diameter at approximately focusing conditions. Smaller beam sizes required excessively longer exposure times. Three angles of X-ray incidence to the disk surface were used in this analysis at each point of stress determination: (1) normal to the surface, (2) 50° to the tangential direction in a normal plane, and (3) 50° to the radial direction in a normal plane. A spot layer of gold filings 0.0035 inch thick was applied to the center of a strip of cellulose tape 0.0025 inch thick, which in turn was applied to the surface of the specimen at each point of stress determination, once each for the three angles of incidence. The X-ray beam was aimed at a 1/32-inch spot of fluorescent powder centered over the gold filings at the desired point on the specimen. The gold was exposed and removed, and the specimen was exposed on the same film. The specimen and the X-ray stand were mounted on separate tables to allow space between them for the swing of the X-ray tube to various positions required by the several angles of X-ray incidence. A dial indicator was attached to the camera base and positioned against a rigid surface on the specimen rigging. Any change in the film-to-specimen distance during exposure of the specimen could thus be readily detected to within 0.0001 inch; if significant change was detected, the two exposures were remade. The tangential- and radial-exposure positions of the camera mounting and gage assembly are shown in figures 4(a) and 4(b), respectively.

Sharp reference lines were scribed on the developed diffraction photographs at right angles to a diameter of the diffraction circles to provide a means of determining the subsequent magnification and to measure diffraction-line diameters of the photographs

on photometer charts. Distances between the reference lines were read to ±0.0002 inch on a microcomparator under a viewing magnification of 4X. Microphotometer scanning along the diameter of the diffraction circles with a potentiometer recorder then produced the chart tracings of X-ray and scribed lines magnified 10X. Diffraction-line peak separations were read on the microphotometer charts and converted to distances on the photographs to an accuracy of ±0.0003 inch. The distance between specimen and X-ray film, the spacing between atomic planes of the specimen, and the stresses in the specimen were then computed from the radii of the various diffraction circles. A photograph of a typical diffraction film is shown in figure 5. The locations of points at which X-ray exposures were made after each spinning are shown in figure 6.

Tangential and radial stresses were calculated from the following equation taken from reference 2 (p. 273):

$$\sigma_{\phi} = \frac{E}{1 + \nu} \frac{1}{\sin^2 \psi} \frac{d_{\psi} - d_{\perp}}{d_{\perp}} \qquad (1)$$

where

σ_{ϕ} stress in either tangential or radial direction, pounds per square inch

E Young's modulus, pounds per square inch

ν Poisson's ratio

ψ angle of X-ray inclination in stress direction to line perpendicular to surface, degrees

d_{ψ} spacing between atomic planes at inclined X-ray incidence, angstroms

$d_{\perp}$ spacing between atomic planes perpendicular to surface, angstroms

The sums of the principal stresses were calculated from the following equation taken from reference 2 (p. 270):

$$\sigma_1 + \sigma_2 = -\frac{E}{\nu} \frac{d_{\perp} - d_0}{d_0} \qquad (2)$$

where

σ_1, σ_2 principal stresses

d_0 spacing between atomic planes perpendicular to surface in stress-free state

The measured sum of the principal stresses was compared with the sum of the individually measured tangential and radial stresses, which are the principal stresses in this case, as a check on the measurement of these individual stresses.

ACCURACY

In the analysis of reference 3, it was concluded that it is possible to estimate from visual observation the position of maximum intensity within a diffraction line with an uncertainty of about 1/10 the width of the line at half maximum intensity. It has been estimated (reference 4) that visual measurement of the films gives about the same accuracy as measurements with a recording microphotometer, namely, 1×10^{-4} A in atomic spacings, for photographs with sharp lines. For diffuse lines the microphotometer is always advantageous. In this work, however, use of a Knorr-Albers microphotometer, which is very accurate, with the precision measuring technique previously described permitted a repetitive accuracy of the measurement of the position of maximum intensity of 1/20 to 1/100 of line width at half maximum intensity as determined by five sets of readings on each of eight lines.

The following equations are derived in reference 3 for calculation of the error in stress measurement by X-ray diffraction:

$$\frac{\delta(d_\psi - d_\perp)}{d_\perp} = 4 \times 10^{-4} \, r \sqrt{2} \qquad (3)$$

where

$\delta(d_\psi - d_\perp)$ probable error in $(d_\psi - d_\perp)$

r probable error in measurement of position of maximum intensity in diffraction line expressed as fraction of width of that line at half maximum intensity

When equation (1) is differentiated, the following expression is obtained:

$$\delta\sigma_{\phi} = \frac{E}{1+\nu} \frac{1}{\sin^2\psi} \frac{\delta(d_{\psi} - d_{\perp})}{d_{\perp}}$$

where

$\delta\sigma_{\phi}$ probable error in σ_{ϕ}

Substitution of equation (3) in the preceding equation gives

$$\delta\sigma_{\phi} = \frac{E}{1+\nu} \frac{1}{\sin^2\psi} r\,(4 \times 10^{-4})\sqrt{2} \qquad (4)$$

Numerical values can then be substituted in equation (4) to yield a minimum value for the probable error in the determination of the principal stresses σ_1 and σ_2

$$\delta\sigma_{\phi} = \frac{10.5 \times 10^6}{1 + 0.34} \frac{1}{(0.642)^2} \frac{1}{20} 4 \times 10^{-4}\sqrt{2}$$

$$= 540 \text{ pounds per square inch}$$

Equations (3) and (4) are based on the assumptions that each crystal grain is a perfect diffractor, that the statistical distribution is uniform, and that the geometric conditions are perfect. The factors that come into play in actual practice, which cause a crystal grain to act as an imperfect diffractor, include the crystal imperfections characterized by the mosaic structure and the displacements of atoms from ideal lattice positions within mosaic domains; the factors that cause nonuniformity in the statistical distribution within the alloy are the non-homogeneity of crystal size, the variation in the concentration and distribution of the alloying elements from crystal to crystal, and nonrandomness of crystal orientation.

In actual practice, repeat measurements were made of the spacing between the (420) planes in the same region on stress-free 3S-0 aluminum without regard to accurate repositioning of the irradiating beam on the same diffracting crystals. As a result, total random changes in $(d_{\psi} - d_{\perp})$ were obtained from this alloy. When these values of $(d_{\psi} - d_{\perp})$ were substituted in equation (1) and the

corresponding stresses were computed, values ranging from ±700 to ±1500 pounds per square inch were obtained. These values include the effect of all variables. These variables may well cause the error in stress measurements to be three times the minimum error as calculated for the ideal case.

In the experimental measurement of the residual stresses discussed in the following section, care was taken to irradiate the same crystals when repeat measurements were made for identification of any stress relaxation. Inasmuch as the diffraction lines of the alloy in the stressed condition appeared to undergo little or no change from the unstressed state, it can be assumed that the error in determining the value of the residual stress at any point is not much larger than ±1500 pounds per square inch. In regions where high stress gradients exist, the error in determining the residual stress at a specified point is further increased by the uncertainity in positioning the apparatus at exactly that point.

RESULTS AND DISCUSSION

Type-A Holding Device

After spinning at 11,500 rpm (type-A holding device), the disk showed slight distortion in a region of about $1\frac{7}{8}$-inch radius, as shown schematically in figure 6(a). This distortion faded slowly, was only slightly visible after 2 weeks, and was invisible after 4 or 5 weeks. The tangential and radial surface stresses measured at the points shown in figure 6(a) are shown in figures 7(a) and 7(b), respectively. The data shown by the solid lines were taken progressively from the hole to the rim over a period of 2 weeks that started at the time the disk was spun. A second series of observations, following the same sequence, was made during the next 2-week period. Large fluctuations in stress, which varied from compressive to tensile, were present within 1/4 inch of the disk hole (radius, 1.38 to 1.65 in.). From 1/4 inch to approximately 1 inch from the hole (radius, 1.65 to 2.38 in.), the stresses, shown by the solid line, changed to a maximum tensile value. For a distance of 1 inch from the hole to the rim, the tangential stresses (fig. 7(a)) remained fairly constant, whereas the trend of radial stress (fig. 7(b)) was toward zero. This trend might have been partly a result of relaxation taking place during the 2-week time interval in which the data were taken along the radius. The tangential stresses in this region varied rather uniformly, whereas the radial stresses showed marked fluctuations. Application of the accuracy of ±1500 pounds per square inch would tend to smooth out these curves, but these fluctuations are often outside the range of this accuracy and therefore must have some validity.

The dashed lines in figure 7, which represent the data taken during the second time period, showed close agreement with the first set of data near the hole. Toward the rim, however, the parallelism became broken by fluctuations. The stress values obtained during the second period either approximated the values obtained during the first 2 weeks or fell below them. The presence of any stress relaxation would indicate that the residual stresses immediately after overspeed may have been slightly higher than those shown by the data points for the solid line. Very often the dashed-line data points fell within the overlap of the accuracy of ±1500 pounds per square inch when it was applied to both the solid- and dashed-line data. The consistently lower stress values for all second-period data presented, with the exception of three data points, as well as the similarity of the changes in the distributions of the stresses after the initial spinning, lend validity to the indication of stress relaxation. Lack of complete parallelism between the solid- and dashed-line curves might be the effect of the non-homogeneous relaxation in adjacent areas. There is, however, no way to confirm this effect completely from the existing data.

Confirmation of the data of these curves is shown in figure 8, in which the independent measurement of the sum of the principal stresses is compared with the sum of the tangential and radial stresses shown in figures 7(a) and 7(b), respectively.

Type-B Holding Device

After the spinning at 10,000 rpm (type-B holding device), which caused a 1/4-inch enlargement of the central hole but no change in the outside diameter, the macrostructure of the disk showed distortion in a central region approximately $2\frac{7}{8}$ inches in radius, as shown in figure 6(b). Well-defined radial strain bands, similar to Lüders' lines in steel, were evident at the periphery of this region with occasional long bands extending toward the rim. These strain bands disappeared rapidly, becoming invisible in 36 to 48 hours.

Visual evidence of the central distortion faded in the manner previously described for the central distortion of the initial spinning. Data were taken on a radius through the largest band as shown (fig. 6(b)) and also on an independent radius over two short arcs, at $2\frac{7}{8}$ and $5\frac{3}{8}$ inches in radius. Figure 9 shows the stress distribution within the long strain band. The disk was stressed, in this case, after an anneal that followed the previous centrifugal straining. The curves are smoother than in the first stressing

at 11,500 rpm (fig. 7). This smoothness is probably the result of more complete elimination of the preferred orientation by the anneal after straining and the fact that the points of stress measurement lie in an area of severe straining. One marked deviation from compressive to tensile stress occurs in the disk at $5\frac{3}{8}$ inches (three-quarters of the disk radius). This deviation was confirmed by remeasurement after 3 weeks. Such high tension might be associated with the coincidence of its location with the tip of the strain band. The marked differences in stress that existed at adjacent points in a region where no marked strain bands were visible to the eye are, however, illustrated in figure 10. This figure shows fluctuations in the stresses between adjacent circumferential points at the radial distance, $5\frac{3}{8}$ inches, at which the high radial tensile stress was noted in figure 9, but on a different radius than that of the strain band. The stresses at $2\frac{7}{8}$ inches of the disk radius on this new radius (fig. 10) are consistent and in fair agreement with those found at $2\frac{7}{8}$ inches of the disk radius in the strain band. The change in the stresses at the two points for which repeated measurements were taken (figs. 9 and 10) compare favorably.

Comparison of Results

The measured stress distributions shown in figures 7 and 8 do not agree closely with the stresses that would be expected on the basis of theoretical plastic-flow determinations such as were made in reference 5 for overspeeded disks. It is possible that the restraining action of the clamp (type-A holding device) on the surface of the disk at a radius of $2\frac{3}{16}$ to $2\frac{3}{8}$ inches produced a residual surface stress that differed from the body stress. This surface restraining action could prevent the surface metal from flowing as freely as the internal material. Although it was observed that plastic flow of the disk had made it slightly thinner by freeing it from restraint by the clamps at the end of the test, initial surface restraint might account for the measured results. Figures 7 and 8 show that the highest tensile stresses apparently fall just outside the radial position of the circumference of the holding clamp. Within this circumference, the stresses fluctuate sharply between tensile and compressive, as if the surface had wrinkled in piling up behind a stationary body. Outside the clamp, all the initially measured residual stresses are tensile. These results then probably do not entirely represent the residual stress within the mass of the disk. This fact is important in its indication of the magnitudes of gradients in stresses than can occur on and in

aircraft-engine components. When an external force (such as encountered in thermal stresses or possibly by velocity impact of exploding or vibrating gases) acts on a metal engine component, the surface stresses may be quite different from those within the component. These surface stresses may therefore be different from the gross stresses existing within the body of the disks and full understanding of the stress distribution must include measurement of surface as well as body stresses.

Data under conditions in which no known outside forces acted on the surface being analyzed are presented in figures 9 and 10. The curves, particularly along a given radius (fig. 9), are more uniform in point-to-point variation than those of figure 8 and may represent the stress condition through the cross section of the disk as well as at the surface. It can be expected, in any case, that the centrifugal force of the tulip petals of the type-B holding device would have some modifying effect on the stress distribution in the disks tested with it. The determination of this effect, however, was not included in this investigation.

SUMMARY OF RESULTS

From an investigation of the residual surface stresses of a parallel-sided 3S-0 aluminum disk with a central hole after plastic strain had been introduced by centrifugal overspeed, the following results were obtained:

1. Locally high stress differences were found superimposed on an over-all trend in the stress curves measured on the surface of a disk overspeeded under conditions at which the surface stresses may have been different from the body stresses. Both the tangential and radial residual surface stresses from centrifugal plastic straining were tensile over the greatest portion of the disk radius even after 3 weeks. Fluctuations between high tensions and high compressions, however, were found in an area adjacent to the central hole.

2. Highly compressive tangential residual stresses near the central hole within a strain band were measured on the surface of a disk overspeeded under conditions at which the surface stresses were probably representative of the body stresses. These stresses were those that remained after the disk was subjected to centrifugal plastic straining by an unbalanced vibratory motion between the edge of the central hole and the driving mechanism. From the hole to the rim the tangential stresses changed from compressive to tensile. The radial stress was compressive except for a highly tensile stress at three-quarters of the disk radius. Fluctuations

were found in tensile stresses between adjacent circumferential points that were also located at three-quarters of the disk radius but on a radius not in the strain band. The stresses at two-fifths of the disk radius on the new radius were consistent and in fair agreement with those found at two-fifths of the disk radius in the strain band.

Flight Propulsion Research Laboratory,
National Advisory Committee for Aeronautics,
Cleveland, Ohio.

REFERENCES

1. Nádai, A.: Plasticity, McGraw-Hill Book Co., Inc., 1931, p. 261.

2. Barrett, Charles S.: Stress Measurements by X-Rays. Structure of Metals, ch. XIV. McGraw-Hill Book Co., Inc., 1943.

3. Ekstein, Hans, and Siegel, Stanley: Limits of Precision in the Determination of Lattice Parameters and Stresses by the Debye-Scherrer Method. NACA TN No. 1375, 1947.

4. Möller, Hermann, und Gisen, Fritz: Ueber die Wiederholbarkeit der Ergebnisse bei der Bestimmung von elastischen Spannungen mit Röntgenstrahlen. Abh. 319, Mitteilungen Kaiser-Wilhelm-Institut f. Eisenforschung Düsseldorf, Bd. XIX, Lfg. 4, 1937, S. 57-59.

5. Millenson, M. B., and Manson, S. S.: Determination of Stresses in Gas-Turbine Disks Subjected to Plastic Flow and Creep. NACA TN No. 1636, 1948.

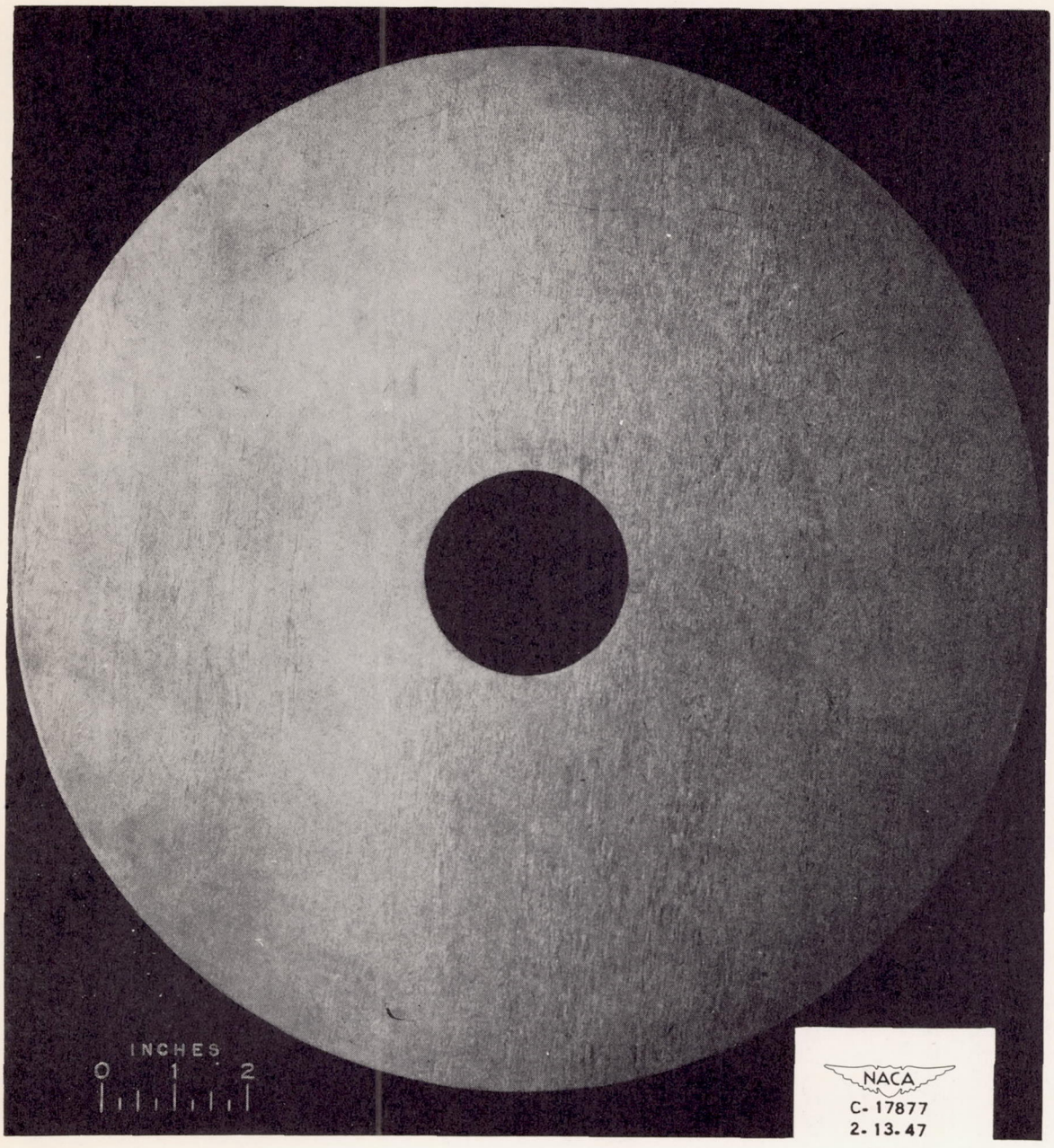

Figure 1. - Macroetched surface of fully annealed 3S-0 aluminum disk before overspeeding.

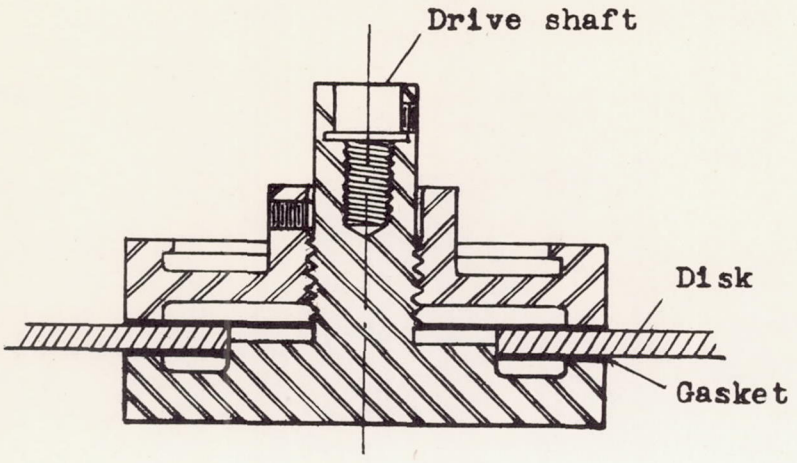

(a) Type A.

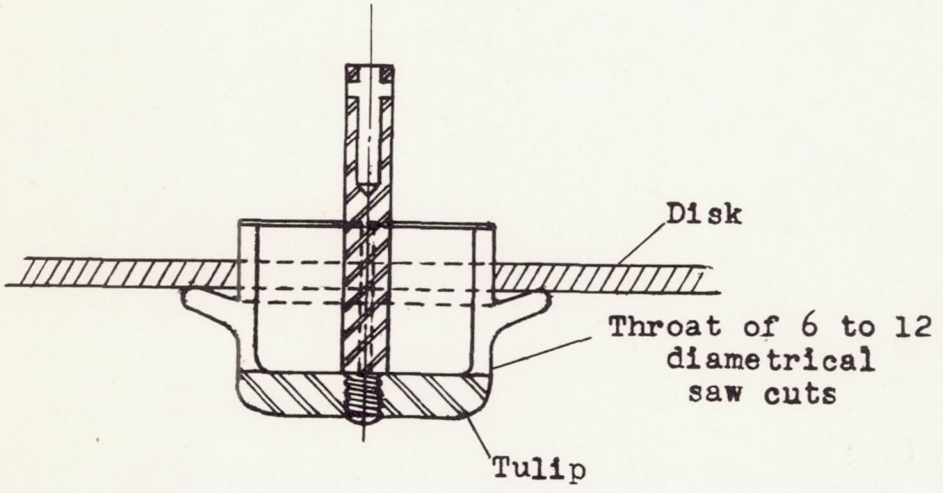

(b) Type B.

Figure 2. - Holding devices for spinning disks.

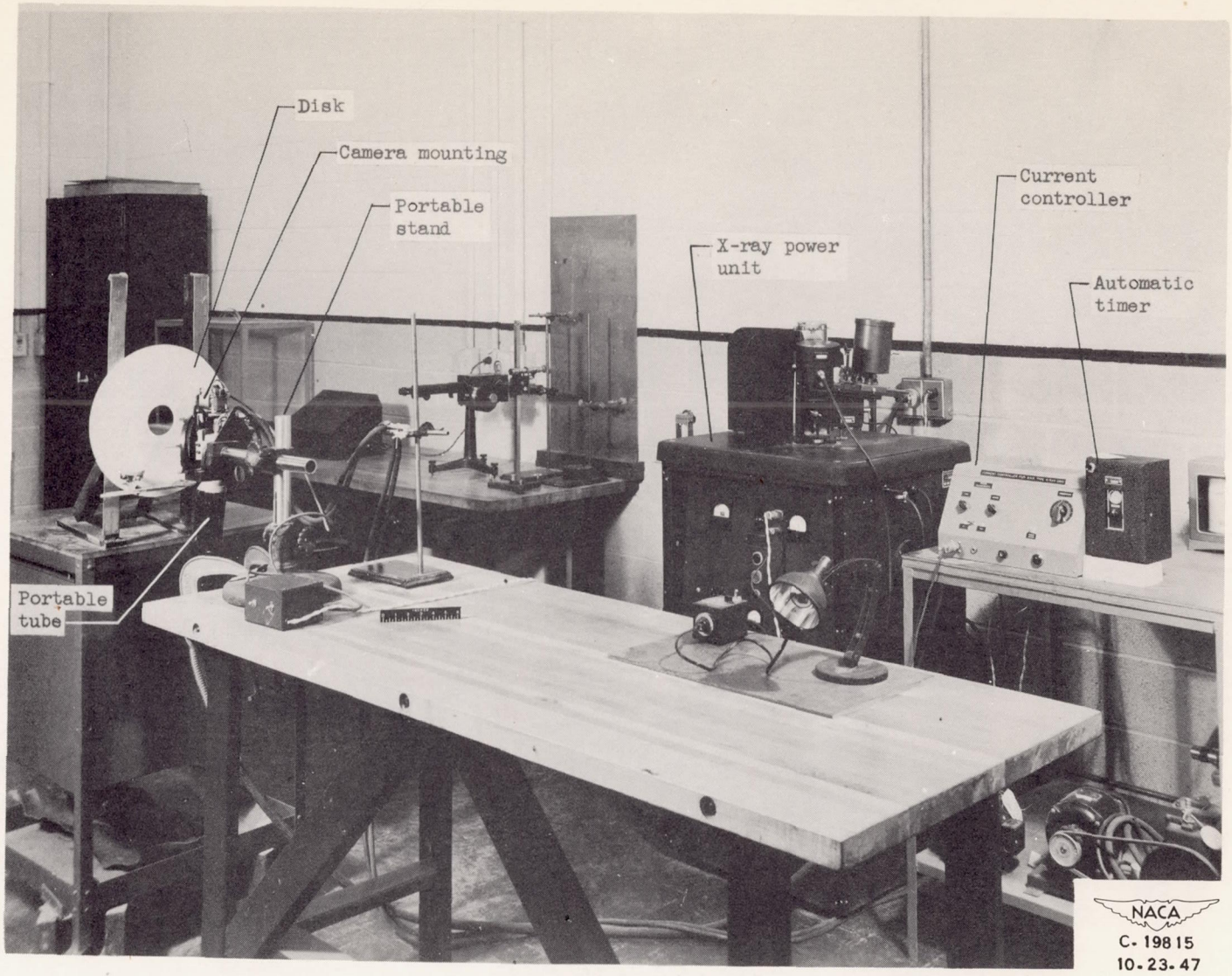

Figure 3. - Laboratory arrangement for photographic X-ray stress analysis.

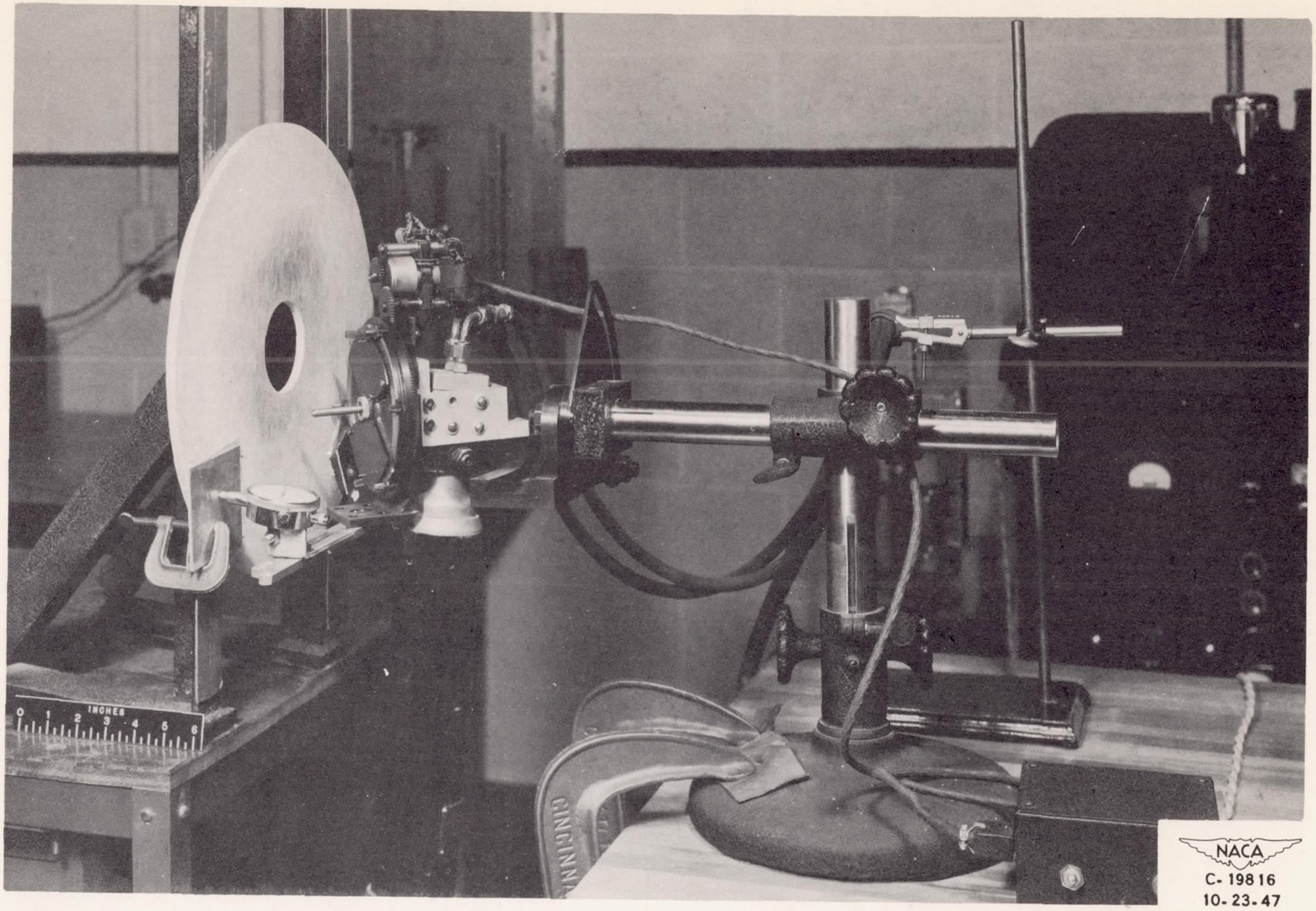

(a) Tangential direction.

Figure 4. - X-ray back-reflection camera and mounting in position for exposure of overspeeded disk.

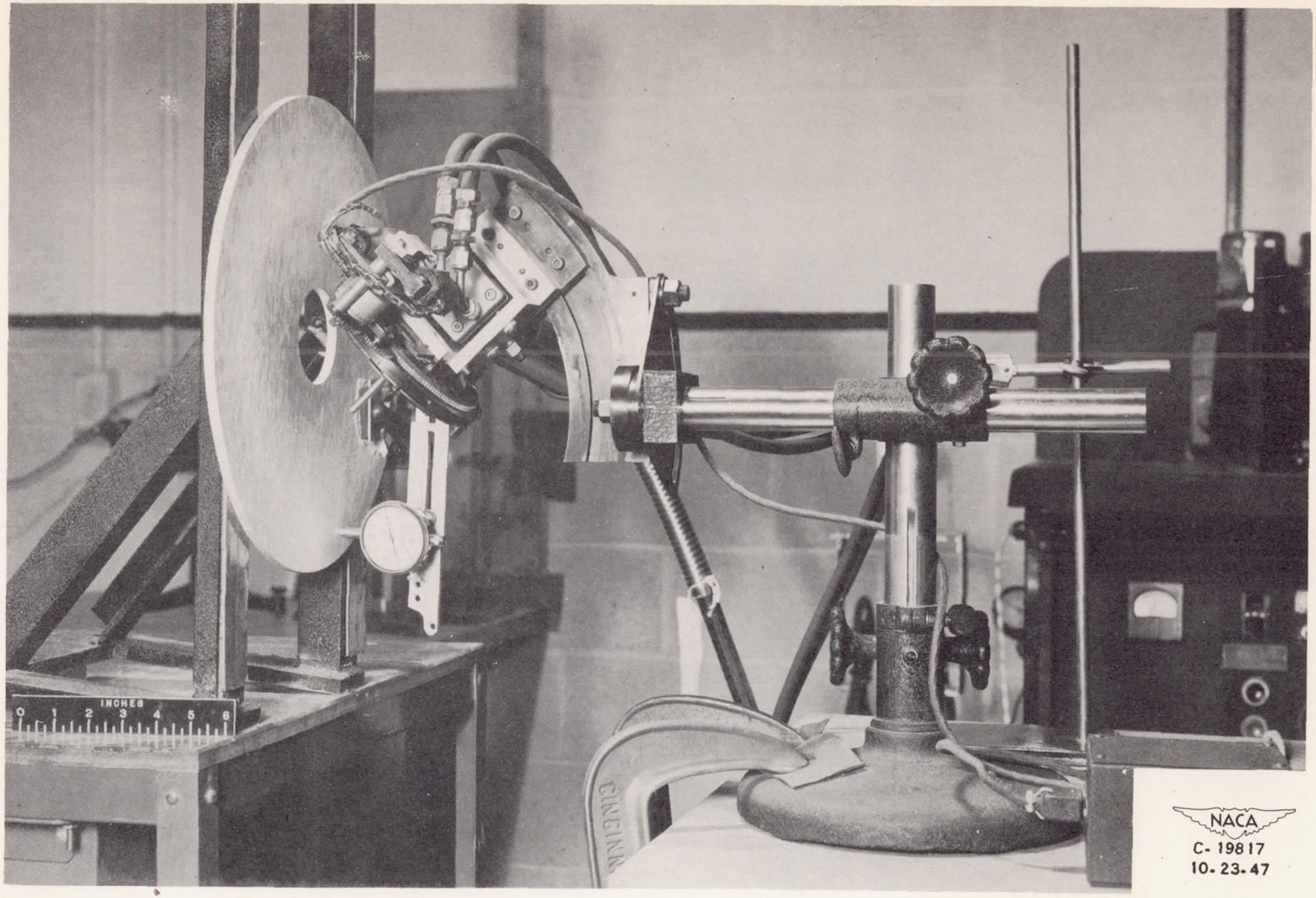

(b) Radial direction.

Figure 4. - Concluded. X-ray back-reflection camera and mounting in position for exposure of overspeeded disk.

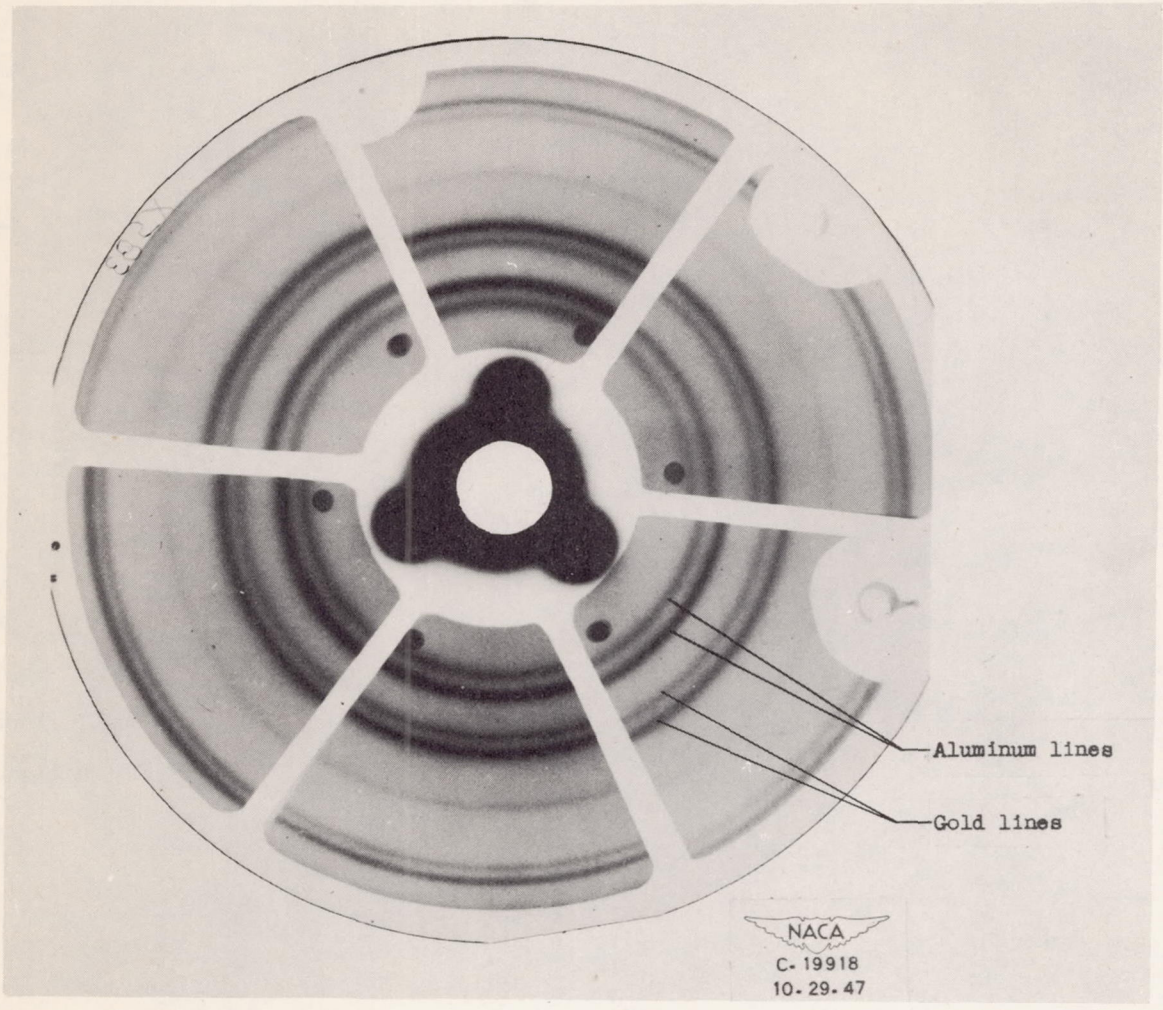

Figure 5. - Characteristic appearance of 3S-0 aluminum and gold standard back-reflection (420) spectral lines.

(a) Maximum disk speed, 11,500 rpm.

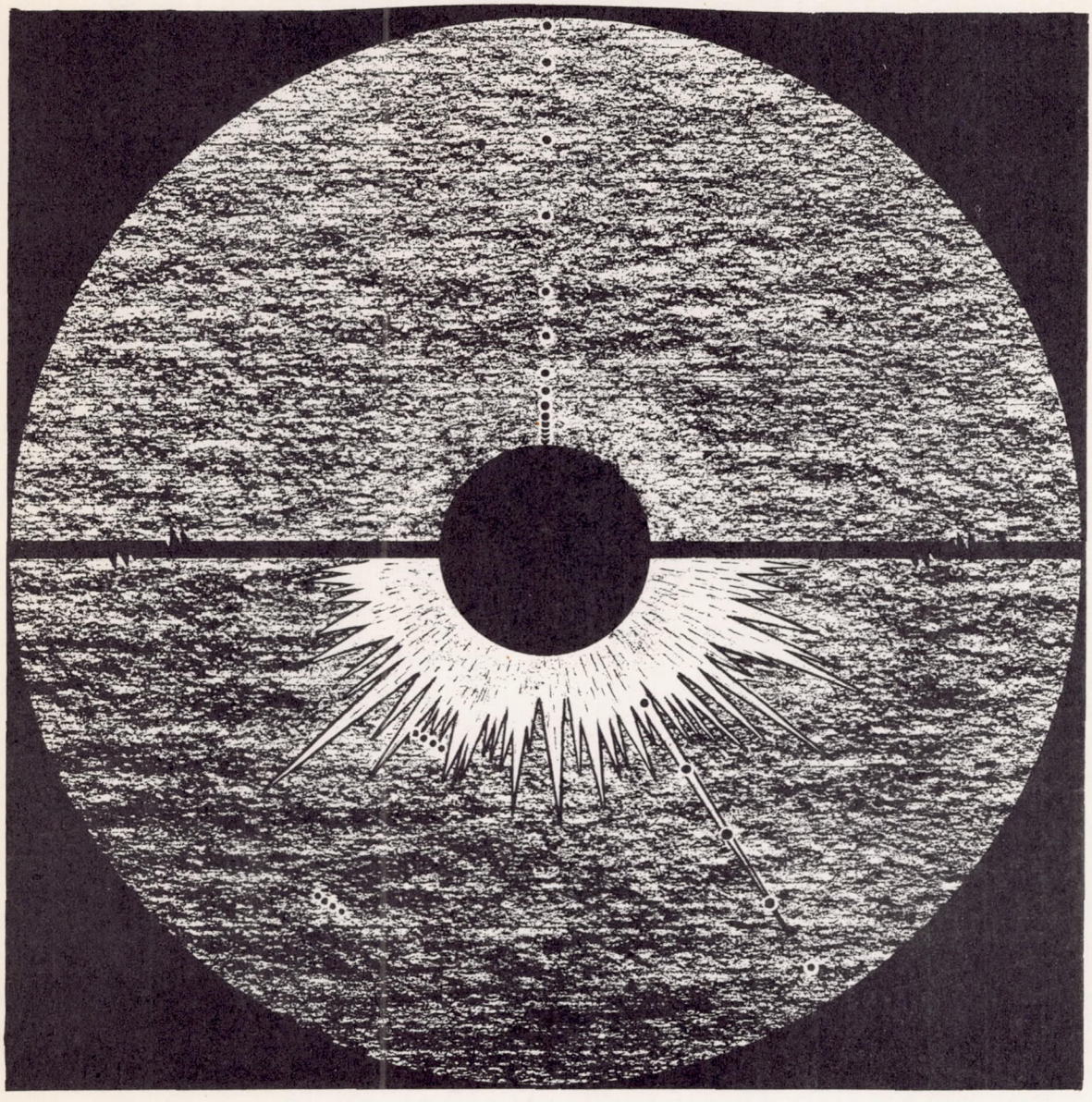

(b) Maximum disk speed, 10,000 rpm.

NACA

Figure 6. - Schematic appearance of 3S-0 aluminum disk after spinning at two maximum disk speeds. Circles show distribution of points of X-ray stress analysis.

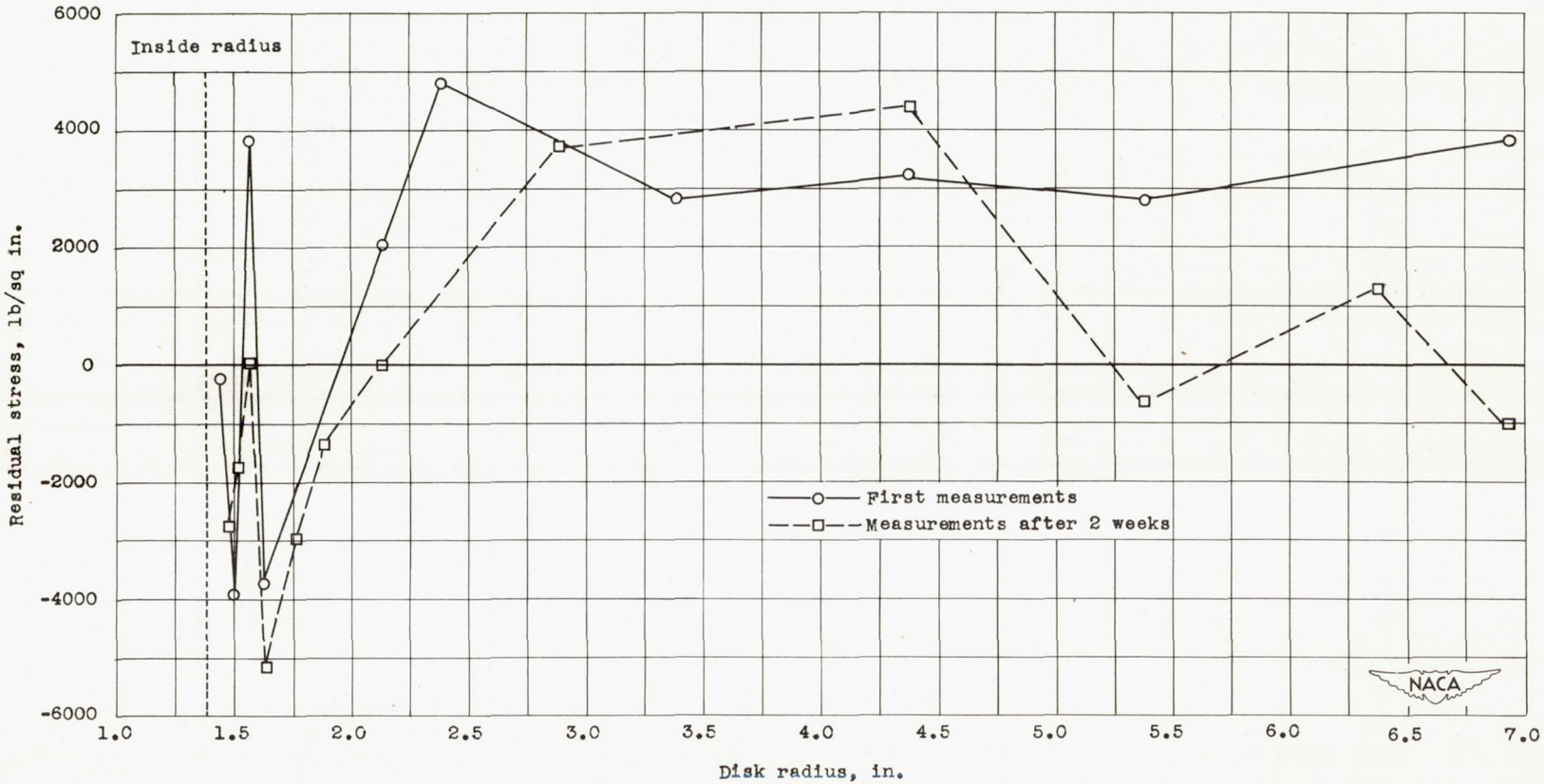

(a) Tangential stress.

Figure 7. - Radial distribution of residual surface stresses on 3S-O aluminum disk spun at 11,500 rpm.

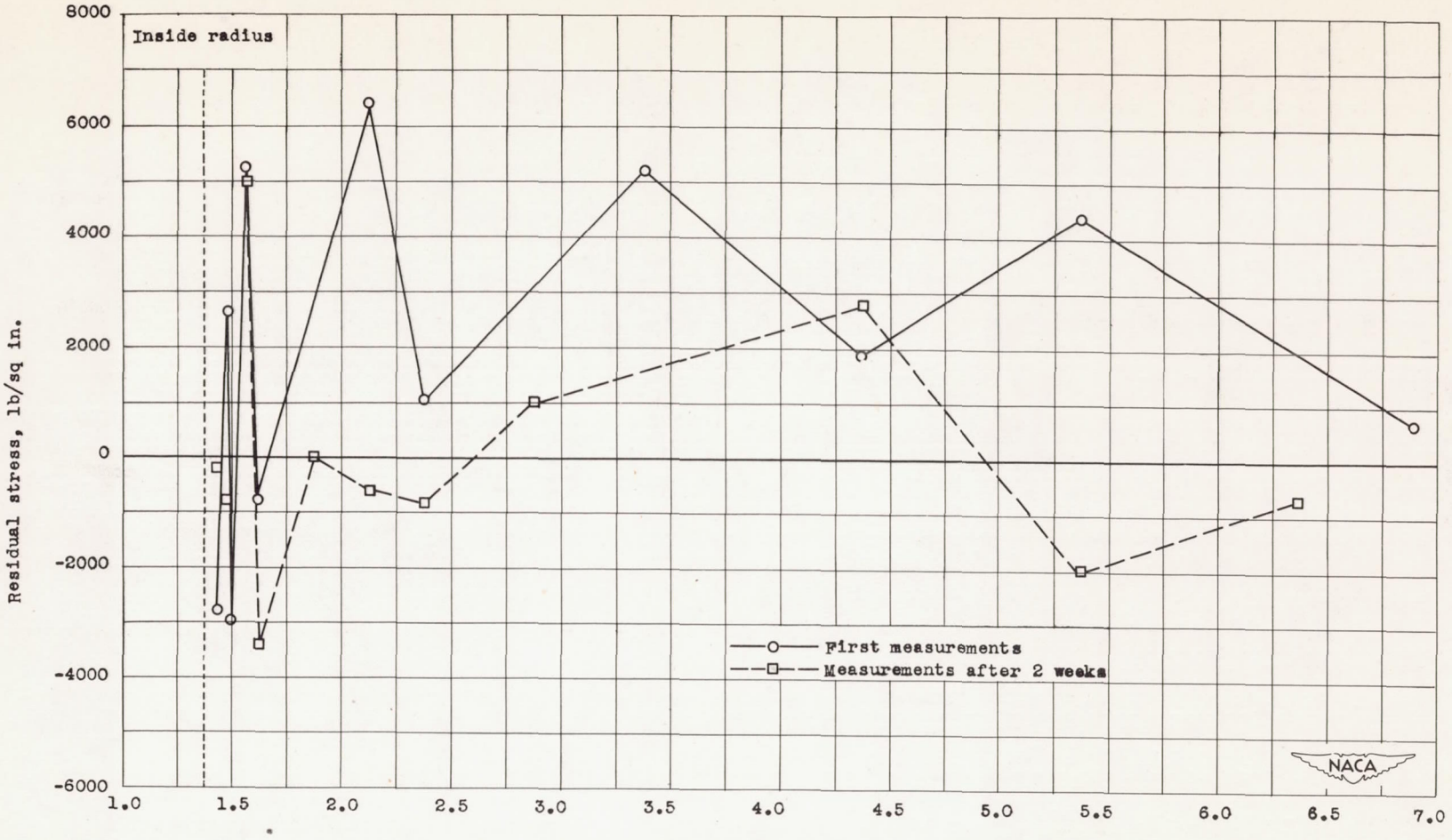

(b) Radial stress.

Figure 7. - Concluded. Radial distribution of residual surface stresses on 3S-0 aluminum disk spun at 11,500 rpm.

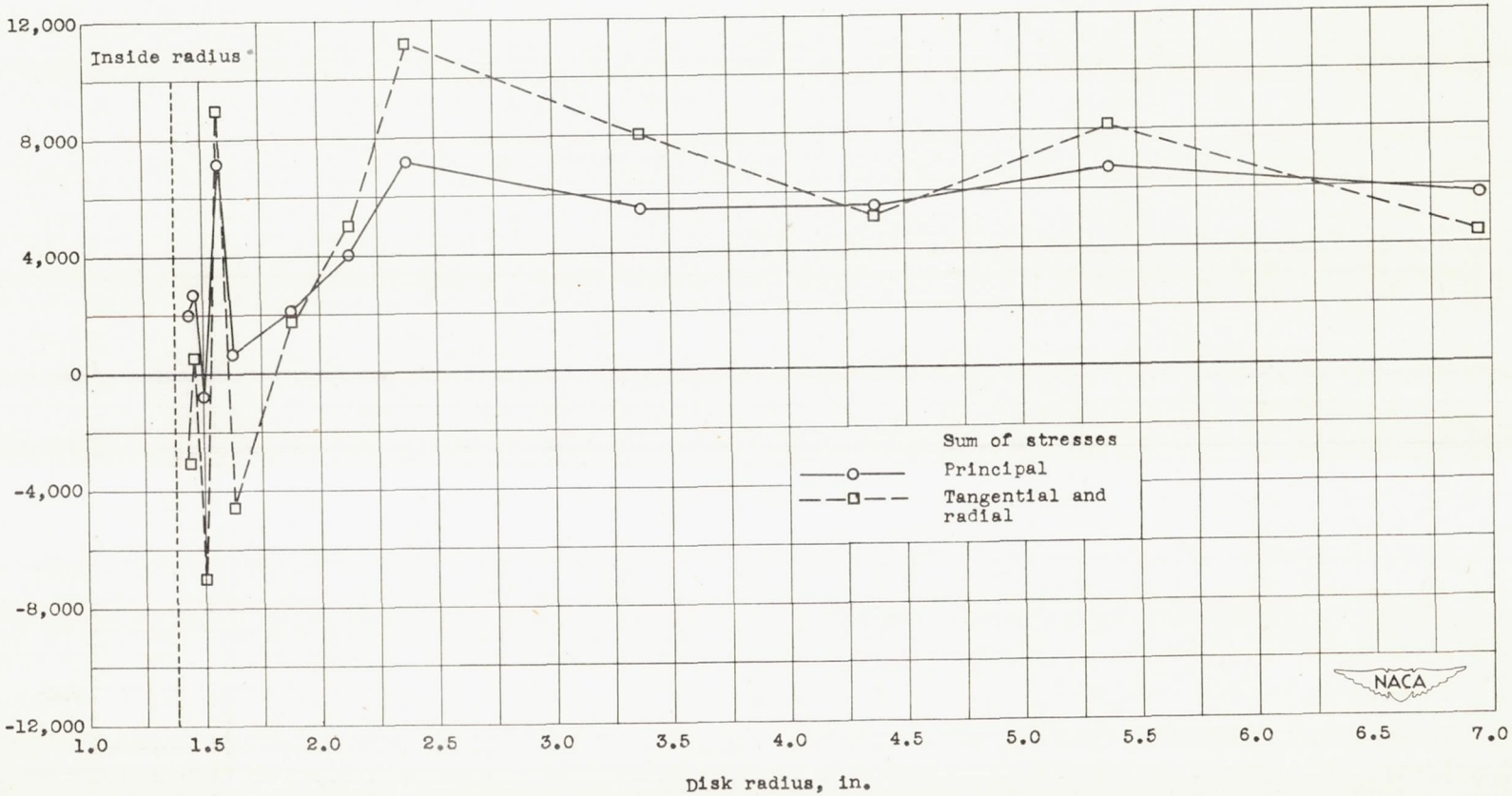

Figure 8. - Comparison of sum of principal surface stresses with sum of tangential and radial stresses on 3S-0 aluminum disk spun at 11,500 rpm.

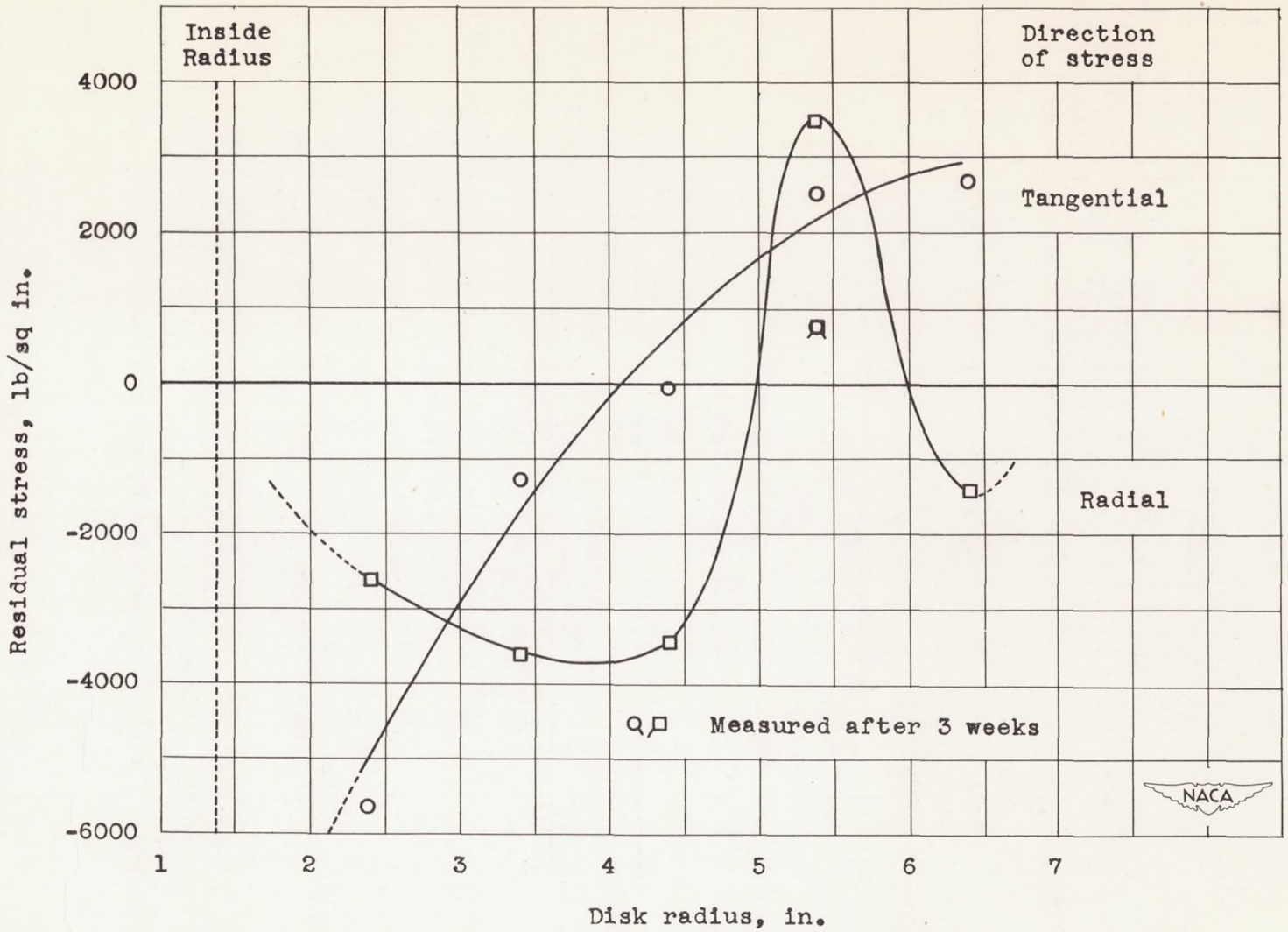

Figure 9.- Radial distribution of residual surface stresses within strain band on 3S-0 aluminum disk spun at 10,000 rpm. Central hole plastically expanded by compression.

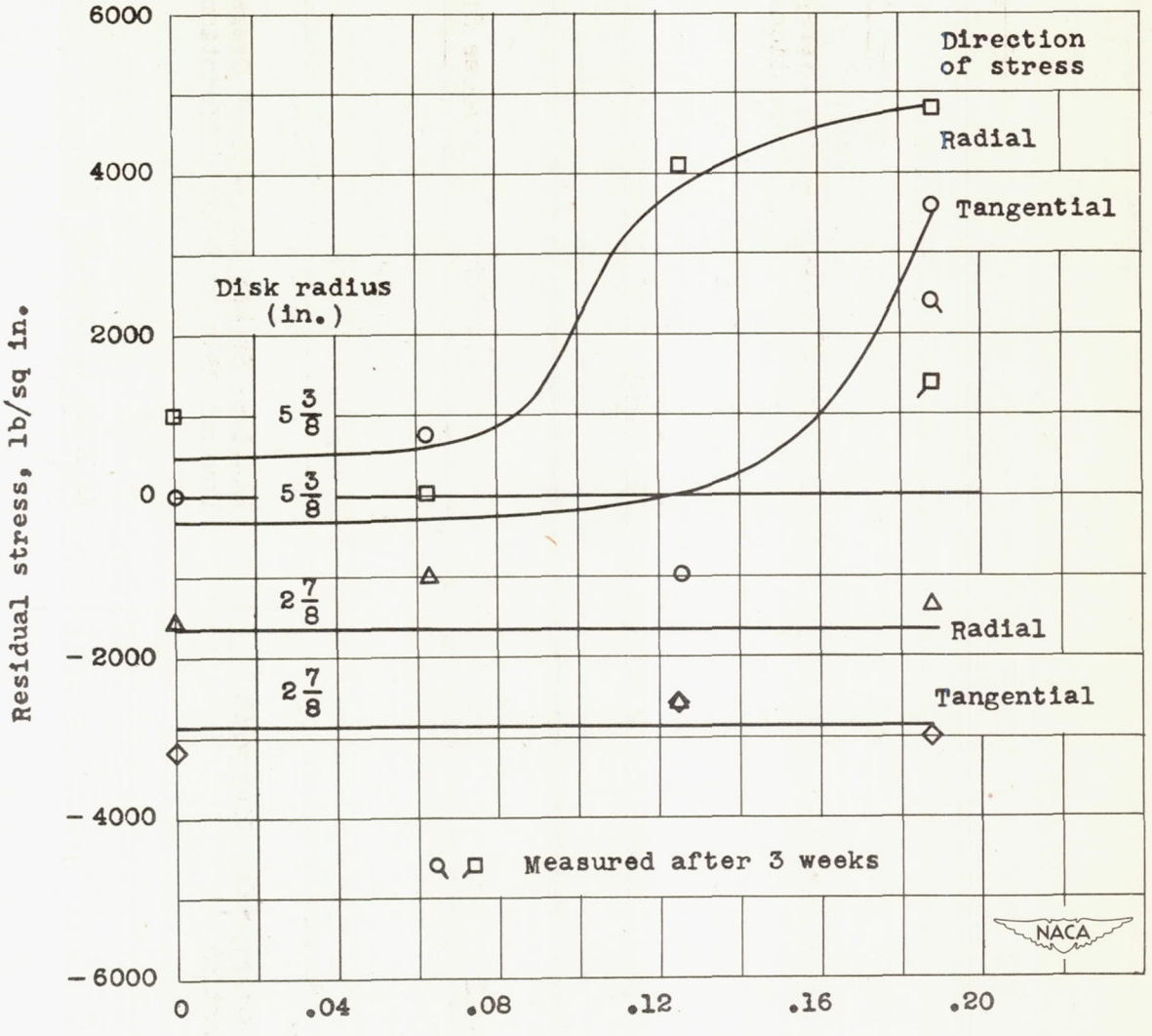

Figure 10. - Circumferential variation of residual surface stresses on 3S-0 aluminum disk spun at 10,000 rpm. Central hole plastically expanded by compression.